Spectrometric and computational studies of the binding of HIV-1 integrase inhibitors to viral DNA extremities

Lea El Khoury [1] , **Krystel El Hage** [2] , **Jean-Philip Piquemal** [3] , **Serge Fermandjian** [4] , **Richard Maroun** [5] , **Nohad Gresh** [Corresp., 6] , **Zeina Hobaika** [5]

[1] Pharmaceutical Sciences, University of California, Irvine, irvine, California, United States

[2] Laboratoire Structure-Activite des Biomolecules, Université d'Evry Val d'Essonne, Evr, Essonne, France

[3] Laboratoire de Chimie Theorique, Université Panthéon-Sorbonne (Paris I), Paris, France

[4] UFR Biomedicale, Université René Descartes (Paris V), Paris, France

[5] Faculte des Sciences, Universite Saint Joseph, Beirut, Lebanon

[6] Laboratoire de Chimie Theorique, Sorbonne Universite, Paris, France

Corresponding Author: Nohad Gresh
Email address: gresh@lct.jussieu.fr

Three Integrase (IN) strand transfer inhibitors are in intensive clinical use, raltegravir, elvitegravir anddolutegravir. However, the onset of IN resistance mutations limits their therapeutic efficiency. As put forth earlier, the drug affinity for the intasome could be improved by targeting preferentially the retroviralnucleobases, which are little, if at all, mutation-prone. We report experimental results of anisotropy fluorescence titrations of viral DNA by these three drugs . These show that the ranking of their inhibitory activities of the intasome corresponds to that of their free energies of binding, D Gs,to retroviral DNA, and that such a ranking is **only** governed by the binding enthalpies, D H, the entropy undergoing marginal variations.This ranking can therefore be directly correlated to that of model Quantum Chemistry (QC) calculations of intermolecular interaction energies of the sole halobenzene ring with the highly conserved retroviral nucleobases G4 and C14, using Density Functional Theory. This DE(QC) ranking is in turn reproduced by the corresponding DE$_{tot}$ values computed with a polarizable molecular mechanics/dynamics procedure, SIBFA (Sum of Interactions Between Fragments Ab initio computed). Such validations should enable polarizable molecular dynamics simulations on more potent inhibitors in their complexes with the complete intasome. Such derivatives should principally encompass modified halobenzene rings.

1

Spectrometric and computational studies of the binding of HIV-1 integrase inhibitors to viral DNA extremities

4

Léa El Khoury [a, b, Ø], Krystel El Hage [b, c, ¥], Jean-Philip Piquemal [a, d, e], Serge Fermandjian [c], Richard G. Maroun [b], Nohad Gresh [a*], and Zeina Hobaika [b*]

[a] Laboratoire de Chimie Théorique, Sorbonne Université, UMR7616 CNRS, Paris 75005, France

[b] UR EGP, Centre d'Analyses et de Recherche, Faculté des Sciences, Université Saint-Joseph de Beyrouth, B.P. 11-514 Riad El Solh, Beirut 1107 2050, Lebanon

[c] Chemistry and Biology Nucleo(s)tides and Immunology for Therapy (CBNIT), UMR 8601 CNRS, UFR Biomedicale, Paris 75006, France

[d] Department of Biomedical Engineering, The University of Texas at Austin, Austin, TX 78712, United States

[e] Institut Universitaire de France, Paris Cedex 05, 75231, France

[Ø] Present address: Department of Pharmaceutical Sciences, University of California, Irvine, California 92697, United States

[¥] Present address: Laboratoire Structure-Activité des Biomolécules Normales et Pathologiques, Université Evry-Val d'Essonne, Evry, France, INSERM, U829, Evry, France.

*Corresponding authors Nohad Gresh (SU), gresh@lct.jussieu.fr; Zeina Hobaika(USJ): zeina.hobaika@usj.edu.lb

38

39 **Abstract.** Three Integrase (IN) strand transfer inhibitors are in intensive clinical use, raltegravir,
40 elvitegravir and dolutegravir. However, the onset of IN resistance mutations limits their
41 therapeutic efficiency. As put forth earlier, the drug affinity for the intasome could be improved
42 by targeting preferentially the retroviral nucleobases, which are little, if at all, mutation-prone.
43 We report experimental results of anisotropy fluorescence titrations of viral DNA by these three
44 drugs. These show that the ranking of their inhibitory activities of the intasome corresponds to
45 that of their free energies of binding, ΔGs, to retroviral DNA, and that such a ranking is **only**
46 governed by the binding enthalpies, ΔH, the entropy undergoing marginal variations. This
47 ranking can therefore be directly correlated to that of model Quantum Chemistry (QC)
48 calculations of intermolecular interaction energies of the sole halobenzene ring with the highly
49 conserved retroviral nucleobases G4 and C14, using Density Functional Theory. This ΔE(QC)
50 ranking is in turn reproduced by the corresponding ΔE_{tot} values computed with a polarizable
51 molecular mechanics/dynamics procedure, SIBFA (Sum of Interactions Between Fragments Ab
52 initio computed). Such validations should enable polarizable molecular dynamics simulations on
53 more potent inhibitors in their complexes with the complete intasome. Such derivatives should
54 principally encompass modified halobenzene rings.

55
56 **I. Introduction.**

57

58 HIV-1 Integrase (IN) is a key element in viral replication. In addition to its essential role in viral
59 DNA (vDNA) integration into host genomic DNA, IN appears involved, directly or indirectly, in
60 reverse transcription [1], nuclear import [2-3] and HIV-1 particle maturation [4-5]. Since in
61 addition IN has no counterpart in human cells, it could represent a privileged target for the
62 design of potent antiretroviral drugs.
63 The integration step is carried by a multimer of INs assembled on vDNA ends, referred to as the
64 intasome. In a first step, denoted as 3'-processing, a 3'GT dinucleotide is removed from each
65 end of the Long Terminal Repeats (LTRs) of vDNA. This occurs in the cytoplasm within a multi-
66 component pre-integration complex (PIC) which gathers the vDNA and several viral and cellular
67 proteins. DNA strand transfer occurs in a second step, after the PIC is chaperoned into the
68 nucleus and results in integration of vDNA as a provirus into the host genome. This requires
69 cutting of two phosphodiester bonds five base pairs apart on opposite strands of the host DNA
70 and is done by free 3'-OH groups that were liberated following LTR processing [6-8].

71   IN strand transfer inhibitors (INSTIs) proved to be much more effective than processing

72   inhibitors and enabled the development of a successful class of antiretroviral drugs [9]. Three

73   inhibitors inspired by the original diketo acids (DKAs) have been successively approved and are

74   commonly used in HIV-1 treatment, namely raltegravir (RAL; MK-0518), elvitegravir (EVG; GS-

75   9137) and dolutegravir (DTG; S/GSK1349572) [10-13]. The latter is a second generation INSTI

76   aimed at maintaining an effective efficacy to IN variants resistant to RAL and EVG [14-15].

77   As was the case for protease and reverse transcriptase inhibitors [16-17], IN inhibitors can

78   generate several resistance mutations. These were recently reported following RAL, EVG and

79   DTG treatment [18-21]. They affect, not only IN residues in direct interactions with INSTIs but

80   also "outer-shell" residues indirectly bound [14, 22-23]. Among these are double mutations such

81   as Q148R/H coupled to G140S/A that produce important synergetic effects on the efficacy of

82   RAL, EVG and even DTG [24-25].

83   EVG, RAL and DTG (Figure 1) selectively bind at the interface of IN and the viral DNA ends,

84   within the intasome and have in common two distinct structural motives: a) a large centralized

85   pharmacophore contributing its keto oxygen and a coplanar neighboring oxygen to coordinate

86   both two IN catalytic Mg(II), structural water molecules, and, either directly or through water, IN

87   residues; and b) a halobenzyl group targeting the highly conserved 5'CpA 3'/5'TpG 3' step on

88   the viral DNA ends [9]. However, the surface and oxygen arrangement of the central

89   pharmacophore differ among the three INSTIs, as well as the nature and position of the

90   halogenation of their terminal aromatic ring: a single F is attached in para to RAL's halobenzene

91   ring, whereas EVG has an F in ortho and a Cl in meta, and DTG has two F atoms in ortho and

92   para.

93   Therefore, within the intasome, the binding of all three drugs targets both viral DNA and the viral

94   protein. In addition to the well-known established interactions with the catalytic and non-catalytic

95   site of IN, following the 3' processing reaction, the X-ray structures of IN-DNA-inhibitor

96   complexes (Figure 1B) show that the halogenated benzene ring stacks over the C base (C14)

97   upstream, while the C-X bond points toward the center of the G base (G4) downstream of the

98   second strand [26-28].

99   On another note, it was reported that, compared with RAL and EVG, DTG displays a more

100   potent *in vitro* anti-HIV activity and a distinct resistance profile [14-15, 29-30]. Furthermore, we

101   have ourselves reported that an increase in the drug-vDNA complex stability correlates with an

102   increase in drug activity and a decrease in viral resistance [14, 27-28], highlighting the important

103   contribution of the vDNA end recognition for the binding affinity of INSTIs to the intasome [31-

104 34]. In this connection, we have shown a narrow correlation between the strongest DTG-DNA
105 affinity and DTG's highest barrier to resistance [32].

106 Maximizing shape complementarity at the IN-vDNA-inhibitor surface could serve as a guiding
107 principle for the development of new INSTIs [9, 26, 31, 35]. An important feature of second
108 generation INSTIS consists into their increased contacts not only with IN active and non-active
109 site, but also with processed viral DNA, right before the strand transfer step. This is supported
110 by the fact that the sequence of the nucleic bases at the ends of the LTR represents stringent
111 requirements concerning retroviral integration and that there is no evidence of mutations in the
112 LTRs that could lead to resistance to INSTIs [35-38].

113

114

115 Could attempts to design novel INSTI's with enhanced affinities focus on the viral DNA, which
116 would render the new inhibitors much less sensitive to mutations occurring on the IN protein?

117 As a continuation of our previous studies, we experimentally measure the ΔG values for the
118 binding of RAL, EVG and DTG to viral DNA. This is done by fluorescence anisotropy
119 experiments at three different temperatures. We also analyze, by both *ab initio* quantum
120 chemistry (QC) and polarizable molecular mechanics/dynamics, the intermolecular interaction
121 energies of their halobenzyl rings with G4 and C14. The individual energy contributions of
122 $\Delta E(QC)$ are also compared to their SIBFA counterparts. Such analyses and validations of
123 inhibitor interactions within the core of vDNA binding site constitute a necessary step toward
124 long-duration PMD of drug-intasome complexes.

125 An outstanding feature of the CX ring in halobenzenes, discovered on the basis of quantum
126 chemistry [39, 40] is the existence of a zone of electron depletion along the extension of the
127 bond with a magnitude increasing along the series F> Cl > Br > I. This 'sigma-hole' goes along
128 with a zone of electronic build-up on a cone around the halogen. It has been earlier shown that
129 atom-centered point charges used in 'classical' force-fields cannot account for the impact of the
130 sigma-hole on the Coulomb electrostatic contribution E_C: this could be only partly remedied
131 upon resorting to an additional fictitious atom prolonging the CX bond with a partial charge and
132 a distance to the X bearer that have to be fit on the basis of QC calculations [41-43] On the
133 other hand, anisotropic potentials such as SIBFA, with distributed atomic multipoles up to
134 quadrupoles, were shown to closely account for the impact of the sigma-hole along the F, Cl,
135 and Br series on the magnitude of E_C both along and around the CX- bond without extra
136 calibration effort [44]. Along these lines, recent work showed that another possibility, resorting to
137 a distributed charge model to reproduce the local quadrupole around the CX could also enable

138   to account for the impact of the sigma-hole on E_C [45, 46] An additional incentive to validate

139   SIBFA in the present work is the perspective of its applications to the entirety of the inhibitor-INT

140   complex, in which the presence of two Mg(II) cations close to one another and of structured

141   water molecules render it preferable to resort to polarizable potentials than to 'classical', non-

142   polarizable ones.

143   At this stage we do not intend to compute true ΔGs to compare the binding affinities of the three

144   inhibitors to vDNA and a fortiori to INT. These would only be meaningful at the outcome of long-

145   duration Molecular Dynamics, and such an outcome could be very sensitive to the accuracy of

146   the intermolecular potential. As a first step toward this evaluation, we focus here on the sole

147   halobenzene-G4/C14 interactions expressed in terms of actual enthalpies of binding and

148   evaluate if two points are satisfied: a) whether the ranking of ΔE(QC) intermolecular interaction

149   energies parallels that of the experimental binding enthalpies; b) whether in turn the

150   corresponding ranking of ΔE(SIBFA) values parallels the QC one.

151

152

153   **II. Materials and Methods**

154

155   **1. DNA sample and inhibitors.** The oligonucleotide LTR32 (Figure 2) was purchased from

156   Eurogentec (Belgium). It was designed to adopt a folded double-stranded hairpin structure even

157   under the low concentrations (10^{-9} to 10^{-5} M) used in fluorescence anisotropy experiments. RAL,

158   EVG and DTG were purchased from AdooQ and Medchemexpress, respectively and their

159   structures are represented in Figure 1A.

160

161

162

163   LTR32 is a linear oligonucleotide sequence designed to adopt a double strand hairpin structure

164   in solution upon folding around a loop created by a purposely added thymine triplet (TTT in

165   green) with the sensitive fluorescein reporter (F, in orange) grafted to its central T. The latter

166   allows fluorescence studies in solution at low concentrations. The stem that reproduces the 3'

167   processed LTR end comprises a 17-nucleotide strand and a 15-nucleotide strand corresponding

168   to the unreactive strand and the reactive strand, respectively. Their pairing leaves an unpaired

169   dinucleotide 5' AC 3' at the 5' end on the unreactive strand. In each strand the nucleotide

170   numbering goes from the 5' to the 3' extremity. The highly conserved doublet of base pairs, here

171   numbered C14-G4 and A15-T3, is colored in red.

172

173   **2. Fluorescence measurements.** Thermodynamic parameters of ligand-processed DNA

174   complexes were identified using fluorescence anisotropy [47-48] on a Jobin-Yvon Fluoromax II

175   instrument. RAL was purchased from AdooQ and EVG and DTG were purchased from

176   Medchemexpress. The LTR32 oligonucleotide, reproducing the processed viral DNA, was

177   purchased from Eurogentec (Belgium). It contains a thymine loop bearing the fluorescein

178   reporter for fluorescence studies. During titrations, labeled DNA (LTR32) was dissolved in

179   phosphate buffer (10mM, pH 6, I=0.1) and placed in thermally jacketed quartz cells (1cm) at

180   5°C, 15°C and 25°C; increasing concentrations of the inhibitors (RAL, EVG or DTG) were then

181   added. The excitation was recorded at 488 nm and the emission at 516 nm. The equilibrium

182   dissociation constants (K_d) were determined with GraphPAD Prism 5 applying the non-linear

183   regression (curve fit)-Least square procedure. This analysis led to the calculation of binding free

184   energies using the following equation: **ΔG= -R T ln (1/k_d).**

185

186   **3. PDB entries.** In the used computational approaches, all complexes were extracted from the

187   X-ray structures of the PFV intasome (IN-viral DNA-Mg^{2+}) in complex with EVG [26] (PDB code:

188   3L2U), DTG [28] (PDB code: 3S3M) and RAL [27] (PDB code: 3OYA).

189

190   **4. Ab-initio QC Computations.** The systems were first energy-minimized at the correlated level

191   using the dispersion – corrected B97-D functional by Grimme et al. [49] and the cc-pVTZ basis

192   set [50, 51] with the Gaussian 9 (G09) software [52].

193   During the minimization C4 and G14 were kept fixed and only the halogenated ring was allowed

194   to move.

195

196   **41. Energy decomposition analysis.** Two sets of calculations were performed at the Hartree-

197   Fock and DFT-d levels in order to obtain all five contributions to the interaction energy.

198

199   **4.1.1. Hartree-Fock (HF) calculations.** The energy decomposition analysis (EDA) was done

200   using the reduced variational space (RVS) procedure of Stevens and Fink [53]. It separates the

201   total interaction energy into four contributions: the first-order (E_1) Coulomb (E_C) and short-range

202   exchange− repulsion (E_{exch}) and the second-order (E_2) polarization (E_{pol}) and charge transfer

203   (E_{ct}). The basis set superposition error (BSSE) [54, 55] is evaluated within the virtual orbital

204   space. EDA was done with the GAMESS software [56] at the HF/cc-pVTZ level of theory. This

205   basis set was shown to closely reproduce the results from the more extended aug-cc-pVTZ

206 basis set in several test calculations bearing on inter- as well as intramolecular interactions [57].

207

208 **4.1.2. Correlated Calculations**. In order to obtain the dispersion contribution, the
209 intermolecular interaction energies ΔE were computed at the correlated level using the
210 dispersion-corrected B97-D functional with the G09 software and the cc-pVTZ basis set. The
211 values of ΔE were also corrected for BSSE. For a given complex, the dispersion contribution
212 (E_{disp}) is evaluated as the difference between the BSSE-corrected B97-D intermolecular
213 interaction energies and the HF ones.

214

215 **5. SIBFA Computations.** The intermolecular interaction energy ($ΔE_{tot}$) is computed as the sum
216 of five contributions: electrostatic multipolar (E_{MTP}), short-range repulsion (E_{rep}), polarization
217 (E_{pol}), charge transfer (E_{CT}), and dispersion (E_{disp}) [58]. E_{MTP} is computed with distributed
218 multipoles derived from the QC molecular orbitals of the individual ligands [59, 60, 61],
219 augmented with penetration [62]. The anisotropic polarizabilities are distributed on the centroids
220 of the localized orbitals [63]. E_{rep} and E_{CT} are computed using representations of the molecular
221 orbitals on the chemical bonds and the lone-pairs. E_{disp} has an expansion into $1/R^6$, $1/R^8$, and
222 $1/R^{10}$ along with an exchange− dispersion component [64]. The parameters for F and Cl were
223 reported in [45].

224

225 **III. Results and discussion.**
226
227 We have previously reported that the strong INSTIs bind tightly to the ends of the 3'-processed
228 vDNA, at the LTR ends [32]; thus, justifying their function as a blocker of the strand transfer step
229 [26]. Table 1 reports the Kd values for the binding of RAL, EVG and DTG to the LTR32
230 oligonucleotide, as determined by fluorescence anisotropy titrations in a phosphate buffer at 5°,
231 15° and 25°C. The fluorescence anisotropy titration curves of LTR32 for increasing
232 concentrations of drugs are reported in Figures S.II., S.III. and S.IV. Those of LTR32 by DTG
233 (S.II.A.) and EVG (S.III.A.) at 5°C already reported in El Khoury et al., 2017 [32], are added to
234 this study for completeness. The DTG > EVG > RAL Kd ranking of inhibitor-vDNA binding
235 affinities is the same, regarding these three inhibitors, as the one reported for their binding to
236 the complete intasome [65]. Including the desolvation energies of the halobenzene rings is not
237 expected to alter this ranking. We have computed their continuum solvation energies $ΔG_{solv}$ with
238 a Polarizable Continuum Model (PCM) [66]. These could represent an upper bound to the 'real'
239 solvation energies, on account of a lesser exposure to solvation of the ring when it is integrated

240 in the entire drug. The present values amount to -5.1, -6.0, and -3.9 kcal/mol for RAL, EVG and

241 DTG, respectively. The relative differences are much smaller than the ΔE_{tot} ones, and their

242 inclusion would actually favor DTG.

243

244

245

246

247 We have further unraveled the enthalpy and entropy components of the free energies of LTR32-

248 INSTI complexation. The ΔG, ΔH and ΔS values are reported in Tables II.a-c.

249

250

251 These results show the affinity ranking of the three inhibitors for end vDNA to be dominated by

252 the enthalpy component. This finding is fully consistent with the microcalorimetry study reported

253 by Chaires et al., which covered 26 DNA ligands [67] and led to the conclusion that formation of

254 DNA-intercalator complexes is enthalpy-driven, while that of DNA-groove binder complexes is

255 entropy-driven. RAL-LTR32, EVG-LTR32 and DTG-LTR32 interactions are characterized by a

256 mean ΔH / ΔG ratio in the 1.3-1.4 range. This is within the 0.83-1.97 ΔH / ΔG ratio range,

257 considered as a signature of an enthalpy-dominated interaction.

258 The above experimental results are an incentive for SIBFA polarizable molecular dynamics

259 simulations of complexes of various halogenated drugs with retroviral DNAs, which should

260 benefit from the massively parallel Tinker-HP software, co-developed in one of our Laboratories

261 [68]. We deemed it necessary, however, to perform a prior validation in addressing the question:

262 to which extent would the binding of the drug halobenzyl rings to G4 and C14 be accountable

263 for the DTG > EVG > RAL ranking, and how well could the outcome from high-level QC

264 computations be accounted for by the SIBFA polarizable molecular mechanics procedure?

265 The considered complexes have small sizes and, for the present purposes, energy-

266 minimizations bore on the sole halobenzyl ring. An evaluation of the SIBFA accuracy is

267 nevertheless mandatory, as there would be little hope that inconsistencies between the SIBFA

268 and QC results at this early stage could be obliterated or restored by subsequent large-scale

269 MD simulations on the entire drug-IN-vDNA complex. It also is in line with our previous analyses

270 on the binding of a series of mono- and poly-halogenated rings to G4/C14 and the sensitivity of

271 ΔE and its individual contributions to diverse chemical substitutions [69, 70]. Table III lists the

272 calculated values of ΔE(QC/B97-D) and ΔE_{tot}(SIBFA). The results are summarized in Table III,

273 which lists the values of ΔE(QC/B97-D) and ΔE_{tot}(SIBFA). Supp. Info SI lists the individual

274   contributions of QC and SIBFA ∆E values and compares their trends. It is first observed that

275   regarding the halobenzene rings, ∆E(B97-D) for the inhibitor-G4-C14 complexes has the same

276   DTG > EVG > RAL ranking as the ∆H values for the DKA-vDNA complexes. This attests to the

277   key role of the halobenzene ring as a modulator of inhibitor affinity for vDNA. It is also noted that

278   the QC results can themselves be closely accounted for by ΔE_{tot}(SIBFA), regarding both the

279   magnitudes of ∆E and the DKA ranking. Close agreements between SIBFA and QC values for

280   the G4/C14 complexes with several halobenzene derivatives were previously reported by us

281   [68]. Supp. Info SI shows that such agreements carry out regarding the individual energy

282   contributions and their trends.

283

284

285

286   **IV. Conclusions and Perspectives**.

287

288   This study focused on three INSTIs successively used in anti-HIV-1 therapy, raltegravir (RAL),

289   elvitegravir (EVG), and dolutegravir (DTG). We carried out measurements of their free energies

290   of binding, ∆G, to the vDNA end in solution, and unraveled their enthalpy and entropy

291   components in solution. We found that the ∆G ranking DTG > EVG > RAL parallels that inferred

292   for the intasome [65]. The ∆G ranking is also paralleled by the ∆H one, a signature for

293   intercalation-driven binding. It is also the same as the one computed by high-level QC for the

294   binding of the halobenzene ring to the sole G4 and C14 dimer, as well as by the SIBFA

295   polarizable molecular mechanics procedure. The consistency between SIBFA and QC was

296   previously supported by the complexes of G4/C14 with a diversity of substituted halobenzenes

297   [69].

298   As put forth in [69], it is possible to leverage the 'Janus-like' properties of the CX bond (X=F, Cl,

299   Br), electron-deficient along the bond and electron-rich in a cone around it, to target respectively

300   and simultaneously electron-rich and electron-deficient sites of the nucleotide bases.

301   Polarizable molecular mechanics is responsive to the electronic changes brought about by

302   substitutions as these impact the magnitude of both QC-derived distributed multipoles and

303   polarizabilities used to compute the E_{MTP}^* and E_{pol} contributions. These should enable to fine-

304   tune and further evolve the affinity of halobenzenes for targeted HIV-1 DNA bases.

305 Along these lines, several novel compounds were recently designed and endowed with more

306 favorable ∆E(QC) and ∆E(SIBFA) values than the DTG ring. They will be reported in a

307 forthcoming paper (El Darazi et al., manuscript in preparation).

308

309 In addition to handling the halobenzene interactions [69, 70], a further asset of SIBFA and

310 related polarizable potentials [71] is the reliable handling of poly-ligated complexes of divalent

311 cations [72] and interactions involving 'discrete' structural waters [73, 74]. Such structural

312 motives are also encountered in the intasome-INSTI complexes.

313

314 Grounded on these validations, we plan to undertake long-duration polarizable MD simulations

315 on a diversity of INSTI complexes with intasome, resorting to the massively parallel computer

316 code Tinker-HP. These will enable to quantify the extent to which the halobenzene-G4/C14

317 interactions are modulated by the conformational flexibilities of each partner within the complex,

318 by the electrostatic potentials and fields exerted by the neighboring INT residues and viral DNA

319 bases, and possibly as well by the two neighboring divalent Mg(II) cations and by the structural

320 waters.

321

322
323
324
325
326 **Figure captions.**

327
328 **Figure 1.** FDA approved Integrase strand transfer inhibitors INSTIs (from left to right):

329 raltegravir, elvitegravir and dolutegravir. (A) 2D structures of the inhibitors. The red dashed

330 circle indicates the halobenzyl moiety. (B) 3D structure of each inhibitor in complex with the

331 Integrase (IN) and the viral DNA (vDNA). (C) Close-up on the interactions involving the

332 halobenzene, cytosine 16 and guanine 14.

333 **Figure 2:** LTR32 is a linear oligonucleotide sequence designed to adopt a double strand hairpin

334 structure in solution upon folding around a loop created by a purposely added thymine triplet

335 (TTT in green) with the sensitive fluorescein reporter (F, in orange) grafted to its central T. The

336 latter allows fluorescence studies in solution at low concentrations. The stem that reproduces

337 the 3' processed LTR end comprises a 17-nucleotide strand and a 15-nucleotide strand

338 corresponding to the unreactive strand and the reactive strand, respectively. Their pairing

339 leaves an unpaired dinucleotide 5' AC 3' at the 5' end on the unreactive strand. In each strand

340   the nucleotide numbering goes from the 5' to the 3' extremity. The highly conserved doublet of
341   base pairs, here numbered C14-G4 and A15-T3, is colored in red.
342
343   **Acknowledgements.**

352
353
354
355
356
357
358
359
360
361
362
363   **IV. References.**
364

365   [1]   Li, X.; Krishnan, L.; Cherepanov, P.; Engelman, A. Structural biology of retroviral DNA
366   integration. *Virology.* **2011,** *411*(2), 194-205.
367   [2]   Engelman, A.; Englund, G.; Orenstein, J.M.; Martin, M.A.; and Craigie, R. Multiple
368   effects of mutations in human immunodeficiency virus type 1 integrase on viral
369   replication. *Virology.* **1995,** *69*(5), 2729-2736.
370   [3]   Ikeda, T.; Nishitsuji, H.; Zhou, X.; Nara, N.; Ohashi, T.; Kannagi, M.; Masuda, T.
371   Evaluation of the functional involvement of human immunodeficiency virus type 1
372   integrase in nuclear import of viral cDNA during acute infection. *Virology.* **2004,** *78*(21),
373   11563-73.
374   [4]   Balakrishnan, M.; Yant, S.R.; Tsai, L.; O'Sullivan, C.; Bam, R.A.; Tsai, A.; Niedziela-
375   Majka, A.; Stray, K.M.; Sakowicz, R.; and Cihlar, T. Non-catalytic site HIV-1 integrase

376   inhibitors disrupt core maturation and induce a reverse transcription block in target
377   cells. *PloS One.* **2013,** *8*(9), p.e74163.

378 [5] Fontana, J.; Jurado, K.A.; Cheng, N.; Ly, N.L.; Fuchs, J.R.; Gorelick, R.J.; Engelman,
379   A.N.; and Steven, A.C. Distribution and redistribution of HIV-1 nucleocapsid protein in
380   immature, mature, and integrase-inhibited virions: a role for integrase in
381   maturation. *Virology.* **2015,** JVI-01522.

382 [6] Bushman, F.D.; Craigie R. Activities of human immunodeficiency virus (HIV) integration
383   protein in vitro: specific cleavage and integration of HIV DNA. *Proc. Natl. Acad. Sci. U.*
384   *S. A.* **1991,** *88*(4), 1339-1343.

385 [7] Pommier, Y.; Johnson A. A.; Marchand C. Integrase inhibitors to treat HIV/AIDS. *Nat.*
386   *Rev. Drug Discovery.* **2005,** *4*(3*)*, 236.

387 [8] Lesbats, P.; Engelman, A.N.; and Cherepanov, P. Retroviral DNA integration. *Chem.*
388   *Rev*. **2016,** *116*(20), 12730-12757.

389 [9] Zhao, X.Z.; Smith, S.J.; Maskell, D.P.; Métifiot, M.; Pye, V.E.; Fesen, K.; Marchand, C.;
390   Pommier, Y.; Cherepanov, P.; Hughes, S.H.; and Burke Jr, T.R. Structure-guided
391   optimization of HIV integrase strand transfer inhibitors. *J. Med. Chem*. **2017,** *60*(17),
392   7315-7332.

393 [10] Grinsztejn, B.; Nguyen, B.Y.; Katlama, C.; Gatell, J.M.; Lazzarin, A.; Vittecoq, D.;
394   Gonzalez, C.J.; Chen, J.; Harvey, C.M.; Isaacs, R.D. Safety and efficacy of the HIV-1
395   integrase inhibitor raltegravir (MK-0518) in treatment-experienced patients with
396   multidrug-resistant virus: a phase II randomised controlled trial. *Lancet.* **2007,**
397   *369*(9569), 1261-1269.

398 [11] Koelsch, K.K.; Cooper, D.A. Integrase inhibitors in salvage therapy regimens for HIV-1
399   infection. *Curr. Opin. HIV AIDS,* **2009,** *4*(6), 518-523.

400 [12] Métifiot, M.; Marchand, C.; and Pommier, Y. HIV integrase inhibitors: 20-year landmark
401   and challenges. *In Advances in pharmacology.* **2013,** *67,* 75-105.

402 [13] Ballantyne, A.D; and Perry, C.M. Dolutegravir: first global approval. *Drugs*. **2013,** *73*(14),
403   1627-1637.

404 [14] Anstett, K.; Brenner, B.; Mesplede, T.; Wainberg, M.A. HIV drug resistance against
405   strand transfer integrase inhibitors. *Retrovirology*. **2017,** *14*(1), 36.

406 [15] Wainberg, M.A.; Han, Y.S. Will drug resistance against dolutegravir in initial therapy ever
407   occur? *Front. Pharmacol.* **2015,** 6, 90.

408 [16] Rhee, S.Y.; Taylor, J.; Fessel, W.J.; Kaufman, D.; Towner, W.; Troia, P.; Ruane, P.;
409   Hellinger, J.; Shirvani, V.; Zolopa, A.; Shafer, R.W. HIV-1 protease mutations and
410   protease inhibitor cross-resistance*. Antimicrob. Agents Chemother.* **2010,** *54*(10), 4253-
411   4261.

412 [17] Tantillo, C.; Ding, J.; Jacobo-Molina, A.; Nanni, R.G.; Boyer, P.L.; Hughes, S.H.;
413   Pauwels, R.; Andries, K.; Janssen, P.A.; Arnold, E. Locations of anti-AIDS drug binding
414   sites and resistance mutations in the three-dimensional structure of HIV-1 reverse
415   transcriptase: implications for mechanisms of drug inhibition and resistance. *J. Mol. Biol.*
416   **1994,** *243*(3), 369-387.

417 [18] Métifiot, M.; Marchand, C.; Maddali, K.; Pommier, Y.; Resistance to integrase inhibitors.
418   *Viruses.* **2010,** *2*(7), 1347-1366.

419 [19] Marinello, J.; Marchand, C.; Mott, B.T.; Bain, A.; Thomas, C.J.; Pommier, Y. Comparison
420   of raltegravir and elvitegravir on HIV-1 integrase catalytic reactions and on a series of
421   drug-resistant integrase mutants. *Biochemistry,* **2008,** *47*(36), 9345-9354.

422 [20] Hazuda, D.J.; Felock, P.; Witmer, M.; Wolfe, A.; Stillmock, K.; Grobler, J.A.; Espeseth,
423   A.; Gabryelski, L.; Schleif, W.; Blau, C.; Miller, M.D.; Inhibitors of strand transfer that
424   prevent integration and inhibit HIV-1 replication in cells. *Science*. **2000,** *287*(5453)*,* 646-
425   650.

[21] Wittkop, L.; Breilh, D.; Da Silva, D.; Duffau, P.; Mercié, P.; Raymond, I.; Anies, G.; Fleury, H.; Saux, M.C.; Dabis, F.; Fagard, C.; Virological and immunological response in HIV-1-infected patients with multiple treatment failures receiving raltegravir and optimized background therapy, ANRS CO3 Aquitaine Cohort. *J. Antimicrob. Chemother.* **2009,** *63*(6), 1251-1255.

[22] Blanco, J.L.; Varghese, V.; Rhee, S.Y.; Gatell, J.M.; Shafer, R.W. HIV-1 integrase inhibitor resistance and its clinical implications. *J. Infect. Dis.* **2011,** *203*(9)*,* 1204-1214.

[23] Chen, Q.; Buolamwini, J.K.; Smith, J.C.; Li, A.; Xu, Q.; Cheng, X.; Wei, D. Impact of resistance mutations.

[24] Goethals, O.; Vos, A.; Van Ginderen, M.; Geluykens, P.; Smits, V.; Schols, D.; Hertogs, K.; and Clayton, R. Primary mutations selected in vitro with raltegravir confer large fold changes in susceptibility to first-generation integrase inhibitors, but minor fold changes to inhibitors with second-generation resistance profiles. *Virology*, **2010.** *402*(2), 338-346.

[25] Naeger, L.K.; Harrington, P.; Komatsu, T.; and Deming, D.; Effect of dolutegravir functional monotherapy on HIV-1 virological response in integrase strand transfer inhibitor resistant patients. *Antivir. Ther.* **2016.** *21*(6), 481-488.

[26] Hare, S.; Gupta, S.S.; Valkov, E.; Engelman, A.; Cherepanov, P. Retroviral intasome assembly and inhibition of DNA strand transfer. *Nature.* **2010,** *464*(7286), 232.

[27] Hare, S.; Vos, A.M.; Clayton, R.F.; Thuring, J.W.; Cummings, M.D.; Cherepanov, P.; 2010. Molecular mechanisms of retroviral integrase inhibition and the evolution of viral resistance. *Proc. Natl. Acad. Sci. U. S. A.* **2010,** *107*(46)*,* 20057-20062.

[28] Hare, S.; Smith, S.J.; Metifiot, M.; Jaxa-Chamiec, A.; Pommier, Y.; Hughes, S.H.; Cherepanov, P. Structural and functional analyses of the second-generation integrase strand transfer inhibitor dolutegravir (S/GSK1349572). *Mol. Pharmacol.* **2011,** mol-111.

[29] Vandekerckhove, L. GSK-1349572, a novel integrase inhibitor for the treatment of HIV infection. *Curr. Opin. Invest. Drugs*. **2010,** *11*(2), 203-212.

[30] Osterholzer, D.A.; Goldman, M. Dolutegravir: a next-generation integrase inhibitor for treatment of HIV infection. *Clin. Infect. Dis.* **2014,** *59*(2), 265-271.

[31] Hobaika, Z.; Zargarian, L.; Maroun, R.G.; Mauffret, O.; Burke, T.R.; and Fermandjian, S. HIV-1 integrase and virus and cell DNAs: complex formation and perturbation by inhibitors of integration. *Neurochem. Res.* **2010,** *35*(6), 888-893.

[32] El Khoury, L.; Piquemal, J.P.; Fermandjian, S.; Maroun, R.G.; Gresh, N.; Hobaika, Z. The inhibition process of HIV-1 integrase by diketoacids molecules: Understanding the factors governing the better efficiency of dolutegravir. *Biochem. Biophys. Res. Commun.* **2017,** *488*(3), 433-438.

[33] Ammar, F.F.; Abdel-Azeim, S.; Zargarian, L.; Hobaika, Z.; Maroun, R.G.; Fermandjian, S. Unprocessed viral DNA could be the primary target of the HIV-1 integrase inhibitor raltegravir. *PLoS One.* **2012,** *7*(7), e40223.

[34] Ammar, F.F.; Hobaika, Z.; Abdel-Azeim, S.; Zargarian, L.; Maroun, R.G.; Fermandjian, S. A targeted DNA substrate mechanism for the inhibition of HIV-1 integrase by inhibitors with antiretroviral activity. *FEBS Open Bio.* **2016,** *6*(4), 234-250.

[35] Hobaika, Z.; Zargarian, L.; Boulard, Y.; Maroun, R.G.; Mauffret, O.; and Fermandjian, S. 2009. Specificity of LTR DNA recognition by a peptide mimicking the HIV-1 integrase α4 helix. *Nucleic Acids Res.* **2009,** *37*(22), 7691-7700.

[36] LaFemina, R.L.; Callahan, P.L.; and Cordingley, M.G. 1991. Substrate specificity of recombinant human immunodeficiency virus integrase protein. *Virology.* **1991,** *65*(10), 5624-5630.

[37] Sherman, P.A.; Dickson, M.L.; and Fyfe, J.A. Human immunodeficiency virus type 1 integration protein: DNA sequence requirements for cleaving and joining reactions. *Virology.* **1992,** *66*(6), 3593-3601.

476 [38] Zargarian, L.; Benleumi, M.S.; Renisio, J.G.; Merad, H.; Maroun, R.G.; Wieber, F.;
477   Mauffret, O.; Porumb, H.; Troalen, F.; and Fermandjian, S. Strategy to discriminate
478   between high and low affinity bindings of human immunodeficiency virus, type 1
479   integrase to viral DNA. *J. Biol. Chem*. 2003, *278*(22), pp.19966-19973.
480 [39] Clark, T.; Hennemann, M.; Murray, J. S.; Politzer, P. Halogen bonding: the sigma-hole.
481   *J. Mol. Mod.* 2007, *13*, 291-296.
482 [40] Politzer, P.; Murray, J. S.; Clark, T. , Halogen bonding: an electrostatically-driven highly
483   directional noncovalent interaction *Phys. Chem. Chem. Phys.* 2010, 12, 7748-7757.
484 [41]   Ibrahim, M. A.; Molecular mechanical study of halogen bonding in drug discovery. *J.*
485   *Comput. Chem.* 2011*, 32,* 2564-2574.
486 [42] Jorgensen, W. L.; Schyman, P. Treatment of Halogen Bonding in the OPLS-AA Force
487   Field: Application to Potent Anti-HIV Agents. *J. Chem. Theory Comput.* 2012, 8, 3895-
488   3901.
489 [43] Kolar, M.; Hobza, P. On Extension of the Current Biomolecular Empirical Force Field for
490   the Description of Halogen Bonds**. *J. Chem. Theory Comput.* 2012, *8*, 1325-1333.
491 [44] El Hage, K.E.; Piquemal, J.P.; Hobaika, Z.; Maroun, R.G.; Gresh, N. 2013. Could an
492   anisotropic molecular mechanics/dynamics potential account for sigma hole effects in
493   the complexes of halogenated compounds?. *J. Comput. Chem.* **2013,** *34*(13), 1125-
494   1135.
495 [45] Devereux, M.; Raghunathan, S.; Fedorov,D. G.; Meuwly, M.. A Novel, Computationally
496   Efficient Multipolar Model Employing Distributed Charges for Molecular Dynamics
497   Simulations. *J. Chem. Theory Comput.* 2014, *10,* 4229-4241.
498 [46] El Hage, K.; Bereau, T.; Jakobsen, S.; Meuwly**, M.** Impact of Quadrupolar Electrostatics
499   on Atoms Adjacent to the Sigma-Hole in Condensed-Phase Simulations**. *J. Chem.*
500   *Theory Comput.* 2016*, 12,* 3008-3019.
501 [47] Heyduk, T.; Lee, J.C. Application of fluorescence energy transfer and polarization to
502   monitor Escherichia coli cAMP receptor protein and lac promoter interaction.
503   *Proc. Natl. Acad. Sci. U.S.A.* **1990,** *87*(5), 1744-1748.
504 [48] Hill, J.J.; Royer, C.A., [19] Fluorescence approaches to study of protein-nucleic acid
505   complexation. In *Methods in enzymology;* Academic Press, 1997; Vol. 278, pp. 390-416.
506 [49] Grimme, S. Semiempirical GGA-type density functional constructed with a long-range
507   dispersion correction. *J. Comput. Chem.* **2006,** *27*(15), 1787-1799.
508 [50] Dunning Jr, T.H. Gaussian basis sets for use in correlated molecular calculations. I. The
509   atoms boron through neon and hydrogen. *J. Chem. Phys.* **1989,** *90*(2), 1007-1023
510 [51] Feller, D., 1996. The role of databases in support of computational chemistry
511   calculations. J. *Comput. Chem.* **1996,** *17*(13), 1571-1586.
512 [52] Frisch, M.J.; Trucks, G.W.; Schlegel, H.B.; Scuseria, G.E.; Robb, M.A.; Cheeseman,
513   J.R.; Scalmani, G.; Barone, V.; Mennucci, B.; Petersson, G.A.; Nakatsuji, H. Gaussian
514   09 Revision D. 01, 2009. *Gaussian Inc. Wallingford CT*. 2009.
515 [53] Stevens, W.J.; Fink, W.H. Frozen fragment reduced variational space analysis of
516   hydrogen bonding interactions. Application to the water dimer. *Chem. Phys. Lett*. **1987,**
517   *139*(1), 15-22.
518 [54] Boys, S.F.; Bernardi, F.D. The calculation of small molecular interactions by the
519   differences of separate total energies. Some procedures with reduced errors. *Mol.*
520   *Phys*. **1970,** *19*(4), 553-566.
521 [55] Simon, S.; Duran, M.; Dannenberg, J.J. How does basis set superposition error change
522   the potential surfaces for hydrogen-bonded dimers?. *J. Chem. Phys.* **1996,** *105*(24),
523   11024-11031.
524 [56] Schmidt, M.W.; Baldridge, K.K.; Boatz, J.A.; Elbert, S.T.; Gordon, M.S.; Jensen, J.H.;
525   Koseki, S.; Matsunaga, N.; Nguyen, K.A.; Su, S.; Windus, T.L. General atomic and
526   molecular electronic structure system. *J. Comput. Chem*. **1993,** *14*(11), 1347-1363.

527 [57] Riley, K.E.; Op't Holt, B.T.; Merz, K.M. Critical assessment of the performance of density
528   functional methods for several atomic and molecular properties. J. Chem. Theory
529   Comput. **2007,** *3*(2), 407-433.
530 [58] Gresh, N.; Cisneros, G. A.; Darden, T. A.; Piquemal, J.-P.,. Anisotropic, polarizable
531   molecular mechanics studies of inter-, intramolecular interactions, and ligand-
532   macromolecule complexes. A bottom-up strategy. *J. Chem. Theory and Comput. 2007*, **3**,
533   1960-1986
534 [59] Stone, A.J. Distributed multipole analysis, or how to describe a molecular charge
535   distribution. *Chem. Phys. Lett*. **1981,** *83*(2), 233-239.
536 [60] Stone, A.J.; Alderton, M. Distributed multipole analysis: methods and applications. *Mol.*
537   *Phys*. **1985,** *56*(5), 1047-1064.
538 [61] Vigné-Maeder, F.; Claverie, P. The exact multicenter multipolar part of a molecular
539   charge distribution and its simplified representations. *J. Chem. Phys.* **1988,** *88*(8), 4934-
540   4948.
541 [62] Piquemal, J.P.; Gresh, N.; Giessner-Prettre, C. Improved formulas for the calculation of
542   the electrostatic contribution to the intermolecular interaction energy from multipolar
543   expansion of the electronic distribution. *J. Phys. Chem. A*. **2003,** *107*(48), 10353-10359.
544 [63] Garmer, D.R.; Stevens, W.J. Transferability of molecular distributed polarizabilities from
545   a simple localized orbital based method. *J. Phys. Chem.* **1989,** *93*(25), 8263-8270.
546 [64] Creuzet, S.; Langlet, J.; Gresh, N. Adjustment of the SIBFA method for potential maps to
547   study hydrogen bonding vibrational frequencies. In *AIP Conference Proceedings*, Vol.
548   239, No. 1, pp. 114-114, October 1991.
549 [65] Hightower, K.E.; Wang, R.; DeAnda, F.; Johns, B.A.; Weaver, K.; Shen, Y.; Tomberlin,
550   G.H.; Carter, H.L.; Broderick, T.; Sigethy, S.; and Seki, T. Dolutegravir (S/GSK1349572)
551   exhibits significantly slower dissociation than Raltegravir and Elvitegravir from wild type
552   and integrase inhibitor-resistant HIV-1 integrase-DNA complexes. *Antimicrob. Agents*
553   *Chemother*. **2011,** AAC-00157.
554 [66] Mennucci, B.; Tomasi, J.; Cammi, R.; Cheeseman, J. R.; Frisch, M. J.; Devlin, F. J.;
555   Gabriel, S.; Stephens, P. J. How the environment controls absorption and fluorescence
556   spectra of PRODAN. A quantum-mechanical study in homogeneous and heterogeneous
557   media. J. Phys. Chem. A. 2002, 106, 6102-6113]
558 [67] Chaires, J.B. A thermodynamic signature for drug–DNA binding mode. *Arch. Biochem.*
559   *Biophys.* **2006,** *453*(1)*,* 26-31.
560 [68] Lagardère, L.; Jolly, L.H.; Lipparini, F.; Aviat, F.; Stamm, B.; Jing, Z.F.; Harger, M.;
561   Torabifard, H.; Cisneros, G.A.; Schnieders, M.J.; Gresh, N.; Tinker-HP: a massively
562   parallel molecular dynamics package for multiscale simulations of large complex
563   systems with advanced point dipole polarizable force fields. *Chem. Sci.* **2018,** *9*(4), 956-
564   972.
565 [69] El Hage, K.; Piquemal, J.P.; Hobaika, Z.; Maroun, R.G.; Gresh, N. Substituent-
566   modulated affinities of halobenzene derivatives to the HIV-1 integrase recognition site.
567   Analyses of the interaction energies by parallel quantum chemical and polarizable
568   molecular mechanics. *J. Phys. Chem. A.* **2014,** *118*(41), 9772-9782.
569 [70] El Hage, K.; Piquemal, J.P.; Hobaika, Z.; Maroun, R.G.; Gresh, N. Could the "Janus-like"
570   properties of the halobenzene CX bond (X☐ Cl, Br) be leveraged to enhance molecular
571   recognition?. *J. Comput. Chem*. **2015,** *36*(4), 210-221.
572 [71] Bell, D.R.; Qi, R.; Jing, Z.; Xiang, J.Y.; Mejias, C.; Schnieders, M.J.; Ponder, J.W.; Ren,
573   P.; Calculating binding free energies of host–guest systems using the AMOEBA
574   polarizable force field. *Phys. Chem. Chem. Phys.* **2016,** *18*(44), 30261-30269.
575 [72] El Khoury, L.; Naseem-Khan, S.; Kwapien, K.; Hobaika, Z.; Maroun, R.G.; Piquemal,
576   J.P.; Gresh, N., Importance of explicit smeared lone-pairs in anisotropic polarizable

577   molecular mechanics. Torture track angular tests for exchange-repulsion and charge
578   transfer contributions. *J. Comput. Chem.* **2017,** *38*(22), 1897-1920.
579   [73]   de Courcy, B.; Piquemal, J.P.; Garbay, C.; Gresh, N. Polarizable water molecules in
580   ligand−macromolecule recognition. Impact on the relative affinities of competing
581   pyrrolopyrimidine inhibitors for FAK kinase. *J. Am. Chem. Soc.* **2010,** *132*(10), 3312-
582   3320.
583   [74]   Gresh, N.; de Courcy, B.; Piquemal, J.P.; Foret, J.; Courtiol-Legourd, S.; Salmon, L.
584   Polarizable Water Networks in Ligand–Metalloprotein Recognition. Impact on the
585   Relative Complexation Energies of Zn-Dependent Phosphomannose Isomerase with D-
586   Mannose 6-Phosphate Surrogates. *J. Phys. Chem. B*. **2011,** *115*(25), 8304-8316.
587
588
589
590

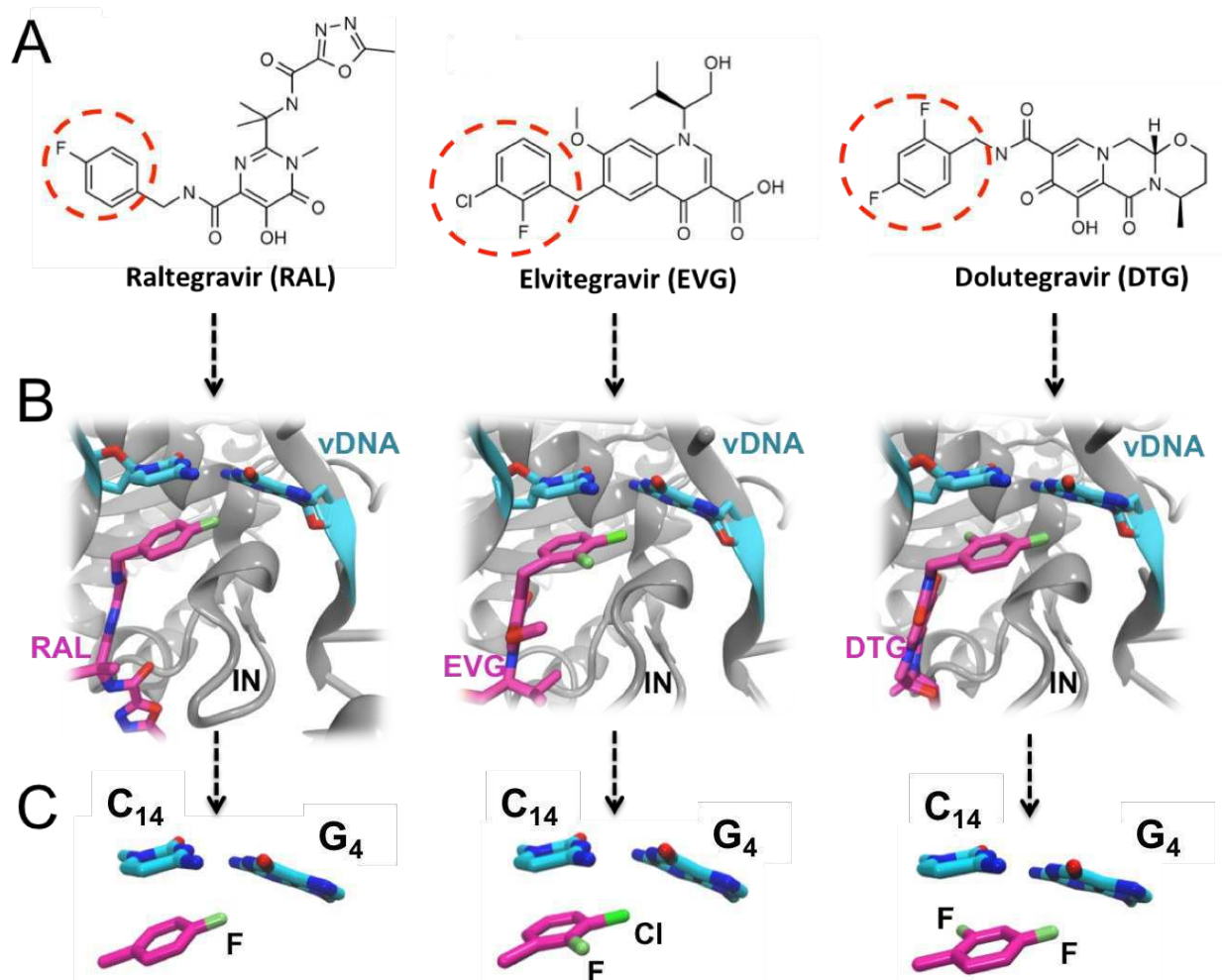**Figure 1**(on next page)

INT Inhibitors

Figure 1. FDA approved Integrase strand transfer inhibitors INSTIs: raltegravir, elvitegravir and dolutegravir. (A) 2D structures of the inhibitors. The red dashed circle indicates the halobenzyl moiety. (B) 3D structure of each inhibitor in complex with the IN active site and the vDNA. (C) Close-up on the interactions involving the halobenzene, cytosine 14 and guanine 4 near the processed 3′-end of the viral DNA.

Figure 2(on next page)

LTR32

```
        1      3  4
5' A C  T G  C T A G A G A T TTT C C  T
                                                T-F
3' HO-A C  G A T C T C T A AAA G G  T
        15 14                              1
```
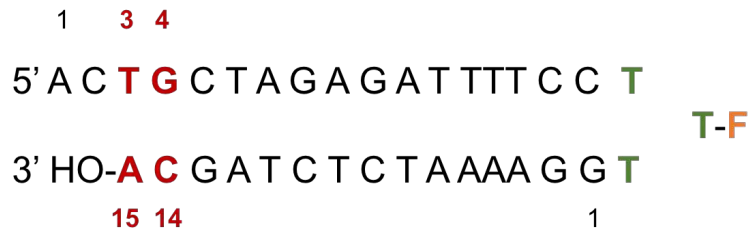
Figure 2: LTR32 is a linear oligonucleotide sequence designed to adopt a double strand hairpin structure in solution upon folding around a loop created by a purposely added thymine triplet (TTT in green) with the sensitive fluorescein reporter (F, in orange) grafted to its central T. The latter allows fluorescence studies in solution at low concentrations. The stem that reproduces the 3' processed LTR end comprises a 17-nucleotide strand and a 15-nucleotide strand corresponding to the unreactive strand and the reactive strand, respectively. Their pairing leaves an unpaired dinucleotide 5' AC 3' at the 5' end on the unreactive strand. In each strand the nucleotide numbering goes from the 5' to the 3' extremity. The highly conserved doublet of base pairs, here numbered C14-G4 and A15-T3, is colored in red.

1

Table 1(on next page)

Dissociation contents of LTR32-INSTI interactions

1

2

Table I. Dissociation constants (Kds) of LTR32-INSTIs interactions			
	RAL	**EVG**	**DTG**
Temperature			
278	5.90E-09	9.50E-11	1.63E-12
288	7.69E-09	1.44E-10	2.74E-12
298	1.26E-08	2.65E-10	6.07E-12
Kd (Molar)			
Temperature (Kelvin)			

3

4

5

6

Table 2(on next page)

Thermodynamic contributions of LTR32-INSTI interactions

1

Table II.a. Thermodynamic contributions of LTR32-raltegravir interaction			
	ΔG	ΔH	TΔS
Temperature			
278	-10.07	-14.16	4.09
288	-10.29	-14.53	4.24
298	-10.37	-14.75	4.39
Values (kcal/mol) of ΔG, ΔH and TΔS			
Temperature (Kelvin)			

Table II.b. Thermodynamic contributions of LTR32-elvitegravir interaction			
	ΔG	ΔH	TΔS
Temperature			
278	-12.27	-16.36	4.09
288	-12.48	-16.71	4.23
298	-12.56	-16.94	4.38
Values (kcal/mol) of ΔG, ΔH and TΔS			
Temperature (Kelvin)			

Table II.c. Thermodynamic contributions of LTR32-dolutegravir interaction			
	ΔG	ΔH	TΔS
Temperature			
278	-14.43	-18.50	4.07
288	-14.66	-18.88	4.22
298	-14.72	-19.08	4.37
Values (kcal/mol) of ΔG, ΔH and TΔS			
Temperature (Kelvin)			

2
3
4

Table 3(on next page)

QC and SIBFA computations of the INSTI(s)=G4/C14 interactions

1

2

Table III. QC and SIBFA computations of the INSTI(s)-C14/G4 interactions.						
	RAL		EVG		DTG	
Procedure	SIBFA	QC	SIBFA	QC	SIBFA	QC
ΔE tot	-31.5	-30.1	-37.1	−38.3	-39.0	-40.8

3

4